Hindawi
Advances in Condensed Matter Physics
Volume 2018, Article ID 9789370, 14 pages
https://doi.org/10.1155/2018/9789370

Research Article

Modification of the Properties of Vanadium Oxide Thin Films by Plasma-Immersion Ion Implantation

Sergey Burdyukh,[1,2] Olga Berezina,[1] and Alexander Pergament[1]

[1]*Institute of Physics and Technology, Petrozavodsk State University, Petrozavodsk 185910, Russia*
[2]*Institute of Geology, Karelian Research Centre, Russian Academy of Sciences, Petrozavodsk 185910, Russia*

Correspondence should be addressed to Alexander Pergament; aperg@psu.karelia.ru

Received 28 October 2017; Accepted 27 December 2017; Published 1 February 2018

Academic Editor: Joseph S. Poon

The paper describes the effect of doping with hydrogen and tungsten by means of plasma-immersion ion implantation (PIII) on the properties of vanadium dioxide and hydrated vanadium pentoxide films. It is shown that the parameters of the metal-insulator phase transition in VO_2 thin films depend on the hydrogen implantation dose. Next, we explore the effect of PIII on composition, optical properties, and the internal electrochromic effect (IECE) in $V_2O_5{\cdot}nH_2O$ films. The variations in the composition and structure caused by the hydrogen insertion, as well as those caused by the electrochromic effect, are studied by nuclear magnetic resonance, thermogravimetry, Raman spectroscopy, and X-ray structural analysis. It is shown that the ion implantation-induced hydrogenation can substantially enhance the manifestation and performance of the IECE in V_2O_5 xerogel films. Finally, the effect of PIII-assisted doping with W on the parameters of electrical switching in $Au/V_2O_5{\cdot}nH_2O/Au$ sandwich structures is examined. It is shown that implanting small tungsten doses improves the switching parameters after forming. When implanting large doses, switching is observed without electroforming, and if electroforming is applied, the switching effect, on the contrary, disappears.

1. Introduction

Vanadium being a transition metal forms a large number of oxide phases with different V atom oxidation degrees: β-phase with an oxygen content of 15 to 25 at.%, γ-phase ($VO_{0.53}$), VO, oxide Magneli phases forming the homologous series V_nO_{2n-1} (including V_2O_3 at $n = 2$), Wadsley phases $V_{2n}O_{5n-2}$, VO_2, and highest oxide V_2O_5. Suboxides VO_x ($x < 1$), monoxide VO, and V_7O_{13} are metallic, while vanadium pentoxide is a dielectric with a bandgap of $E_g \sim 2.35$ eV. A remarkable property of many other vanadium oxides is that they exhibit metal-insulator transitions (MIT) as functions of temperature [1–3].

In stoichiometric VO_2 single crystals, the MIT occurs at a temperature of 340 K. It is a first-order phase transition: a latent heat of 4.27 kJ/mol is absorbed at heating and released at cooling; there is a temperature hysteresis whose width ΔT_t varies from 0.5 to 20 K, and the crystal lattice volume changes at the phase transition [1]. The jump in the electrical conductivity σ during the transition reaches five orders of magnitude. At a temperature above T_t, VO_2 is a "bad metal" (like, e.g., high-T_c superconductors in the normal state and some other metallic oxides of transition and rare-earth elements [4]). Below T_t, the material exhibits semiconductor properties with $E_g \sim 0.7$ eV, but the $\sigma(T)$ dependence does not comply with the Arrhenius law because of the polaron hopping conductivity contribution [5]; the VO_2 semiconductor phase is a correlated (Mott) insulator [2, 6].

In addition, in MOM structures with vanadium dioxide, as well as in structures based on some other transition metal oxides, the phenomenon of electrical switching associated with MIT is observed [7]. The switching effect is a sharp, significant, and reversible change in the system conductivity under the action of the applied electric field. Doping VO_2 with various metals and hydrogen allows one to control the value of T_t [1, 7–10] and, accordingly, the S-shaped *I-V* characteristic parameters, for example, the threshold voltage V_{th}. On the other hand, the study of the MIT in vanadium dioxide, doped with hydrogen or metals with a

valence greater than 4 (e.g., W^{6+}), is of great importance from the viewpoint of further understanding the transition mechanism. The point is that a transformation of the crystal structure, accompanied by the lattice period doubling along the rutile unit cell C_r axis, occurs in VO_2 at the transition. This fact would seem to make it possible to consider the MIT in this material as a structural Peierls transition [1] with the charge density wave formation. Meanwhile, there exists a large amount of experimental data that support the Mott electron-correlation transition scenario [2, 6, 8–10] as the MIT initiating mechanism in vanadium dioxide. In this context, doping, which leads to an increase in the free carrier concentration, is an effective way to either confirm or refute the hypothesis of the Mott transition in vanadium dioxide [8–10].

Vanadium pentoxide demonstrates electrochromic behavior under lithium or hydrogen intercalation due to the formation of $Li_xV_2O_5$ or $H_xV_2O_5$ bronzes [11, 12].

The electrochromic effect has potential applications in making optical indicators, displays, optoelectronic switches, sensors, and so on. In the hydrated vanadium pentoxide $V_2O_5{\cdot}nH_2O$ (n = 1.6–1.8), the internal electrochromic effect (IECE) is observed without the use of an external electrolyte [13].

The IECE in vanadium pentoxide xerogel takes place when a DC voltage is applied to the film across the two metal electrodes. At the flowing current, a bright red spot appears and gradually grows under the negative electrode. This phenomenon is associated with the migration of protons, which are present in the xerogel water phase, toward the cathode and formation of red-colored highest polyvanadic acids, particularly, hexavanadic $H_4V_6O_{l7}$ or decavanadic $H_6V_{10}O_{28}$ acid inclusions, inside the vanadium pentoxide layers [13]. Accordingly, one can suppose that the effect might be enhanced by means of an additional saturation of the $V_2O_5{\cdot}nH_2O$ film by hydrogen. Therefore, doping the vanadium pentoxide xerogel films with hydrogen appears also to be an urgent problem.

Moreover, electrical switching is observed in MOM structures based on vanadium pentoxide gel films after electroforming which results in formation of a VO_2 channel inside the film between metal electrodes [7, 8]. It has been shown that doping of the initial $V_2O_5{\cdot}nH_2O$ film with tungsten allows minimization of the statistical spread (which is an inevitable consequence of the electroforming process) of the V_{th} value [7, 8]. This minimization is surely important for practical applications of vanadium oxide switches [7].

All the foregoing allows us to conclude that the alloying of vanadium oxide films is of undoubted interest, since it provides an opportunity for varying the MIT and switching parameters in a wide range, as well as for the improvement of the IECE manifestation and performance in V_2O_5 xerogel films.

Current methods of alloying, particularly those based on thermal-diffusion processing, have a disadvantage associated with an inhomogeneous distribution of the dopant. In addition, thermal-diffusion doping requires substantial heating of the sample. Doping at the stage of synthesis (e.g., with magnetron sputtering using a V-W target or the introduction of tungsten oxide into the initial sol in the production of films by the sol-gel method) also results in an inhomogeneous distribution of impurities and even phase separation. The ion-beam implantation method requires high ion energies, while the penetration depth of alloying elements in the material is unacceptably high, and the ion-beam implantation systems themselves require complex beam focusing and sample movement devices, so implantation at low energies and small depths of doping becomes ineffective. In addition, both ion-beam and heat treatment can be accompanied by a change in oxygen stoichiometry, in particular, by oxidation of VO_2 to higher oxides of the $V_{2n}O_{5n-2}$ series or by reduction of vanadium pentoxide or vanadium dioxide to lower oxides of the V_nO_{2n-1} series. The method of plasma-immersion ion implantation (PIII) [14], applied in the present work for the doping of thin films of vanadium oxides, lacks these drawbacks. At the PIII processing, the sample is placed directly into the low-temperature plasma, and implantation is performed immediately over the entire surface of the sample. This leads to a uniform implantation over a large area with a rapid gaining of the necessary dose (and, hence, the dopant concentration), while the treatment process proceeds at a low temperature. The doping homogeneity depends only on the plasma uniformity above the sample surface, and the energy of the implanted ions can be varied from unities to hundreds of keV.

Thus, the modification of the properties of vanadium oxide films during their doping by the method of plasma-immersion ion implantation is a topical task. In this paper we report the results of the effect of doping with hydrogen and tungsten by means of plasma-immersion ion implantation on the structure, composition, and physical properties of vanadium dioxide and hydrated vanadium pentoxide films. The metal-insulator transition, electrochromic effect, and electrical switching in these materials are studied, and their modification under doping is examined.

2. Methods and Materials

2.1. Plasma-Immersion Ion Implantation. In the case of doping with hydrogen, the samples were hydrogenated using a specially designed PIII setup schematically depicted in Figure 1(a). The setup included a working chamber with a sample holder ("target" in Figure 1(a)), vacuum system, plasma generator, high-voltage pulse system, and gas supply system. The working chamber had the shape of a cube made of vacuum stainless steel with a working volume of $400 \times 400 \times 400$ mm^3. A hot-cathode plasma source (HCPS) was attached to one of the working chamber flanges. The HCPS initiated an arc discharge in the working chamber. The vacuum system based on a turbomolecular pump ensured the residual gas pressure in the chamber as low as 10^{-4} Pa. Voltage pulses were applied to the sample holder via an HVS-10-10 solid-state switch. The gas (hydrogen) supply system consisted of two FC-260 gas flow controllers.

The irradiation dose N (number of ions incident on a unit target area) was estimated from the following expression

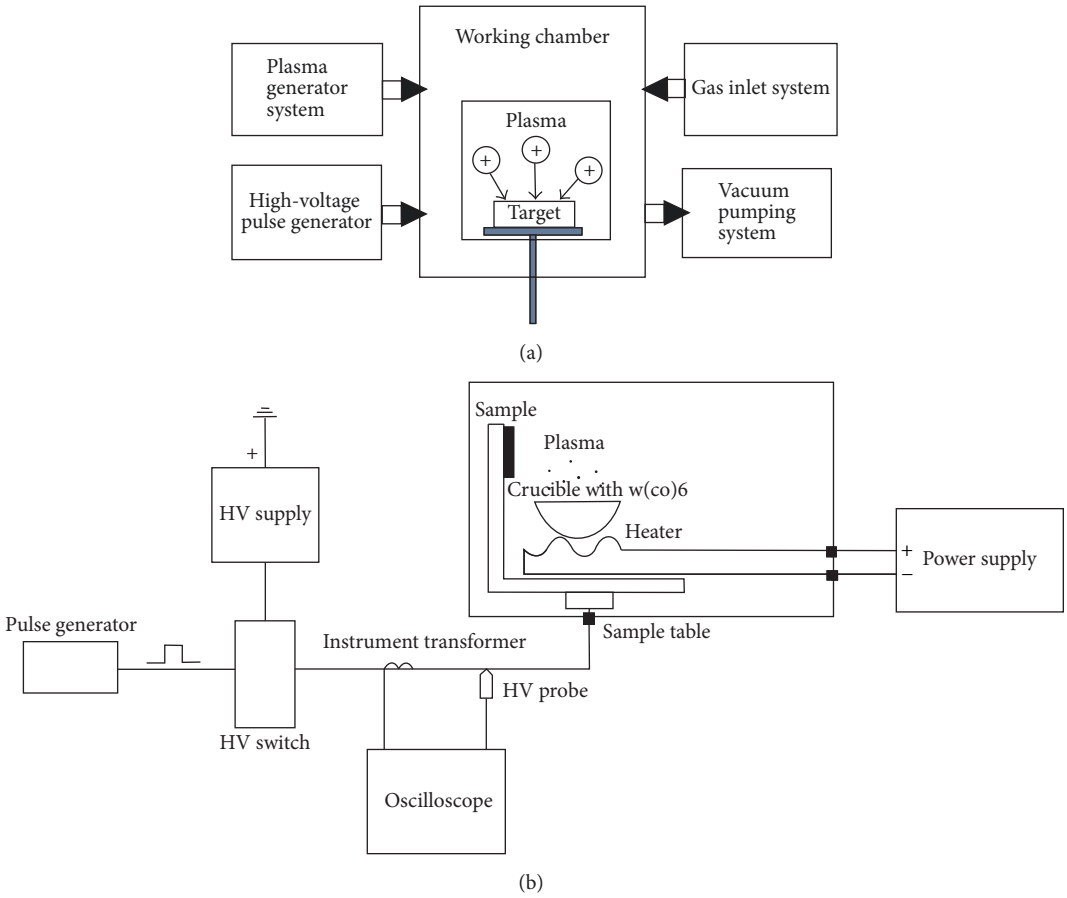

Figure 1: (a) Block diagram of PIII setup and (b) the setup modification for W implantation.

based on the magnitude of current flowing through the sample:

$$N = \frac{I_{\text{imp}} \cdot \Delta t \cdot \nu \cdot t}{e \cdot s}, \quad (1)$$

where I_{imp} is the current pulse amplitude, Δt is the pulse duration, ν is the pulse repetition rate, t is the overall processing time, $e = 1.6 \times 10^{-19}$ C is the H^+ ion charge, and S is the sample area.

The parameters of PIII are presented in Table 1. For V_2O_5 gel films, the irradiation dose was determined from (1), and the doses used in the experiments were varied in the range $(1.0–3.5) \cdot 10^{17}$ cm^{-2}. In some experiments, only a half of the film was hydrogenated, while a mask covered another half. The film region exposed to the hydrogen implantation, that is, the hydrogenated region, changed its color from yellow-brown or gray-green to dark-green.

When implanting tungsten, the discharge was ignited in argon. A crucible with tungsten hexacarbonyl $W(CO)_6$ was placed into the working chamber and heated up to 200°C (Figure 1(b)). The melting point of $W(CO)_6$ is 169°C, and the boiling point is 175°C. At $T = 200$°C tungsten hexacarbonyl sublimates in vacuum, and $W(CO)_6$ vapor appears in the discharge chamber.

Molecules $W(CO)_6$ are ionized in the discharge and implanted into the sample.

The gas composition during the experiment was monitored with a quadrupole mass spectrometer Thermo Scientific DSQ II. From the mass spectra (Figure 2), we determined the partial pressures of Ar and $W(CO)_6$ indicated in Table 1.

It should be noted that the dose of tungsten implantation could not be determined from the current value according to (1), inasmuch as argon ions contributed to the total current too. Therefore, the W concentration in the films after PIII was evaluated from the energy dispersive X-ray (EDX) spectra obtained using a Hitachi SU 1510 scanning electron microscope.

2.2. Sample Preparation and Characterization. Film samples of 200 nm thick polycrystalline vanadium dioxide VO_2 on glass-ceramic substrates were fabricated using an AJA ORION 5 setup by reactive magnetron sputtering in a mixture of argon and oxygen (the partial pressures of Ar and O_2 were 4.3 and 0.7 Torr, and the DC generator power was 200 W) with subsequent annealing at a temperature of 500°C.

The $V_2O_5 \cdot nH_2O$ films were obtained by the sol-gel method [8, 13, 15]: the vanadium pentoxide powder was placed in an alundum crucible and kept in a muffle furnace for 1 hour at a temperature of 900°C. After that, the V_2O_5

Table 1: Parameters of plasma-immersion ion implantation.

Parameter, unit	Implantation of H into VO_2	Implantation of H into V_2O_5 gel	Implantation of W into V_2O_5 gel
Discharge current, A	9.5	9	10
Discharge voltage, V	69.5	75	55
Cathode heating current, A	65	60	65
Pressure, Pa	4	4	1.2 (Ar); 3.8 ($W(CO)_6$)
Gas flow, m^3Pa/s	0.0018 (H_2)	0.0018 (H_2)	0.0018 (Ar)
V_{imp} applied to sample, kV	2	2	2
I_{imp}, mA	20	50	50
Δt, μs	10	10	5
t, min	1–5	5–30	1–5
ν, kHz	1-2	2	1.7

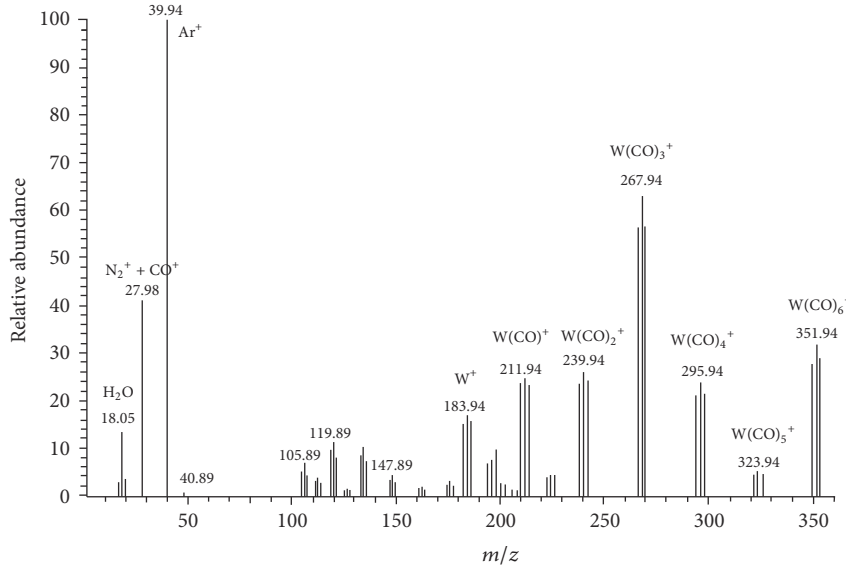

Figure 2: : Mass spectrum of gas in the experimental chamber when the crucible with $W(CO)_6$ is heated.

melt was poured into distilled water and the resulting solution was thoroughly mixed. Subsequent to aging and filtration, the obtained gel was deposited onto glass substrates by the dip-coating method. After drying, films with a thickness of less than 1 μm had a gray-green color, and thicker films (1-2 μm) were yellow-brown. The film thickness was estimated using a KEYNCE VK-9710 confocal laser scanning microscope by the scratch depth.

The samples were characterized by X-ray diffraction (XRD) analysis, optical (VIS-NIR) spectroscopy, dispersive Raman spectrometry, nuclear magnetic resonance (NMR) spectroscopy, and thermal gravimetric analysis (TGA).

The XRD analysis was carried out using a DRON-3 diffractometer with CuKα radiation (wavelength 1.5418 Å), and a pyrolytic graphite monochromator was installed in the reflected beam. The measurements were conducted over the angular range $2\theta = 2^\circ$ to 145° with the step of 0.1°, and the time of shooting of each point was 15 seconds. The optical reflectance $R(\lambda)$ and transmittance $T(\lambda)$ spectra were measured with an SF-56 spectrophotometer in the wavelength range of 300–1100 nm. The Raman analysis of the samples was made using a Nicolet Almega XR Dispersive Raman spectrometer with the reference beam of 532 nm in Raman shift spectral range of 100–1500 cm^{-1}. The ^1H (400.1 MHz) and ^{51}V (105.2 MHz) MAS NMR spectra were obtained using a Bruker AVANCE-II 400 WB spectrometer equipped with a 4 mm H/X MAS probe. For both nuclei, the Hahn echo sequence "90°-τ-180°-τ- acquisition" with a sample rotation frequency of 14 kHz was used. Echo delay τ was equal to 1 rotor rotation period. Number of scans and relaxation delays were 64 and 2 s for ^1H and 2048 and 0.5 s for ^{51}V, respectively. The TGA of vanadium oxide xerogel films was performed using a Hitachi High-Tech Sciences STA7300 High Temperature Simultaneous Thermal Analyzer. The sample was heated to 100°C and then held at this temperature for half an hour, that is, for the time of hydrogen implantation in plasma. Further, to determine the total amount of water in the $V_2O_5 \cdot nH_2O$ sample, it was heated up to 400°C (the temperature at which all the bound water was removed from $V_2O_5 \cdot nH_2O$ and vanadium pentoxide crystallized [15]) and held at this temperature for some time.

The conductivity temperature dependence of VO_2 films was measured using the four-point probe method. The temperature was measured with a chromel–alumel thermocouple

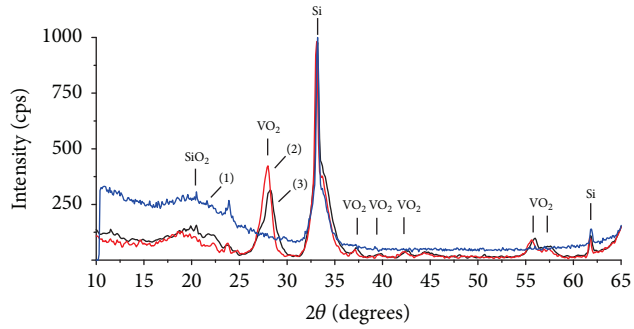

Figure 3: XRD patterns of Si substrate (1), initial VO_2 film on silicon (2), and VO_2 film after hydrogen implantation.

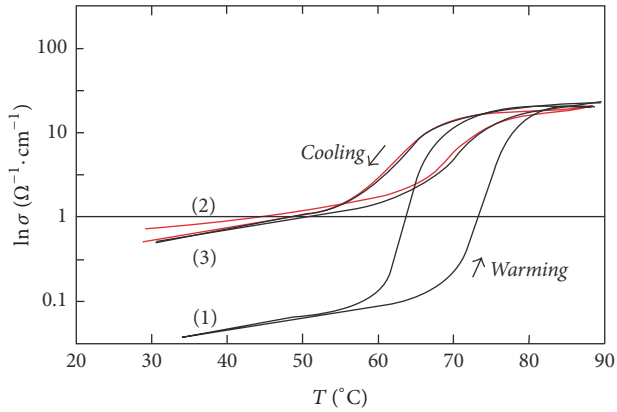

Figure 4: Conductivity temperature dependence of VO_2 film: initial sample 1 (1), region of the film with implanted hydrogen (2), and the same region, second measurement (3). The implanting dose is $7.5 \cdot 10^{15}$ cm^{-2}, and the time of one 30–90–30°C thermal cycling is about 1 hour.

and a Keithley 2000 multimeter. The voltage and current at probes were measured by a Keithley 2400 sourcemeter.

For the manifestation of the IECE in $V_2O_5{\cdot}nH_2O$ films, a constant DC voltage of about 30 V was applied to the film using point spring-loaded electrodes located at a distance of 3 mm from each other. The red spot (similar to that shown in Figure 1 of our previous work [13]) growing around the negative electrode was photographed at regular intervals, and the spot area was then calculated from the photographs.

The switching effect was studied in a sandwich-type structure Au-$V_2O_5{\cdot}nH_2O$-Au on the basis of vanadium oxide xerogel films, both pure and doped with W, obtained by the sol-gel method. Electroforming (EF) of the switching structures was carried out by a Keithley 2400 sourcemeter in the current limiting mode, and the EF voltage was 30 V.

3. Results and Discussion

3.1. Vanadium Dioxide. The XRD analysis (Figure 3) revealed that the obtained films represented vanadium dioxide. In the experiment, the films were heated to about 100°C by radiation from the HCPS hot cathode. Thus, vanadium dioxide in the metallic tetragonal phase was subjected to hydrogenation. The coefficient of hydrogen diffusion in this phase is considerably higher than that in the semiconductor monoclinic phase [16]. In Figure 3, a wide peak of about 20° refers to the substrate and most likely corresponds to the amorphous phase of SiO_2, which is formed upon heating during implantation.

Figures 4 and 5 show the conductivity temperature dependence of the VO_2 films before and after hydrogen implantation with different doses. Sample 1 (Figure 4) has been subjected to hydrogen implantation for 1 min at a pulse repetition rate of 1 kHz. According to formula (1), the irradiation dose is $N = 7.5 \times 10^{15}$ cm^{-2} in this case. The concentration of hydrogen in the VO_2 film is equal to 3.7×10^{20} cm^{-3}; that is, the doping level is 1.2 at.%. The conductivity jump falls by an order of magnitude (curve (2) in Figure 4) as compared to the initial film (curve (1)), and the MIT temperature also decreases. The duration of one $\sigma(T)$ measurement is about 1 hour; for this time, the hysteresis loop shape is slightly altered from one measurement to another (curve (3) in Figure 4). This suggests that hydrogen is gradually removed from the film during the conductivity measurements [17].

In the work [18], the hydrogenation of vanadium dioxide films has been performed in hot glycerine. When this hydrogenation technique is applied, hydrogen is retained within films for only a short time (several tens of minutes); that is, almost all hydrogen escapes from the film in the process of $\sigma(T)$ measurements. When PIII hydrogenation is used, hydrogen is retained within films for several days. The films are heated in the process of measurements, and the rate of hydrogen escape is increased relative to that at

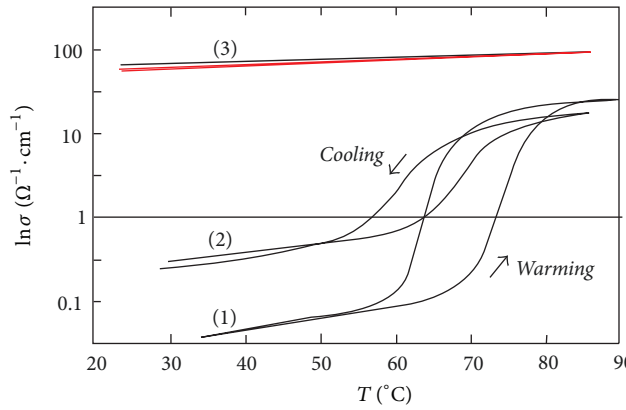

FIGURE 5: Conductivity temperature dependence of VO_2 film: initial sample 2 (1), the region covered by a mask (2), and region with implanted hydrogen (3). The implanting dose is $7.5 \cdot 10^{16}$ cm^{-2}.

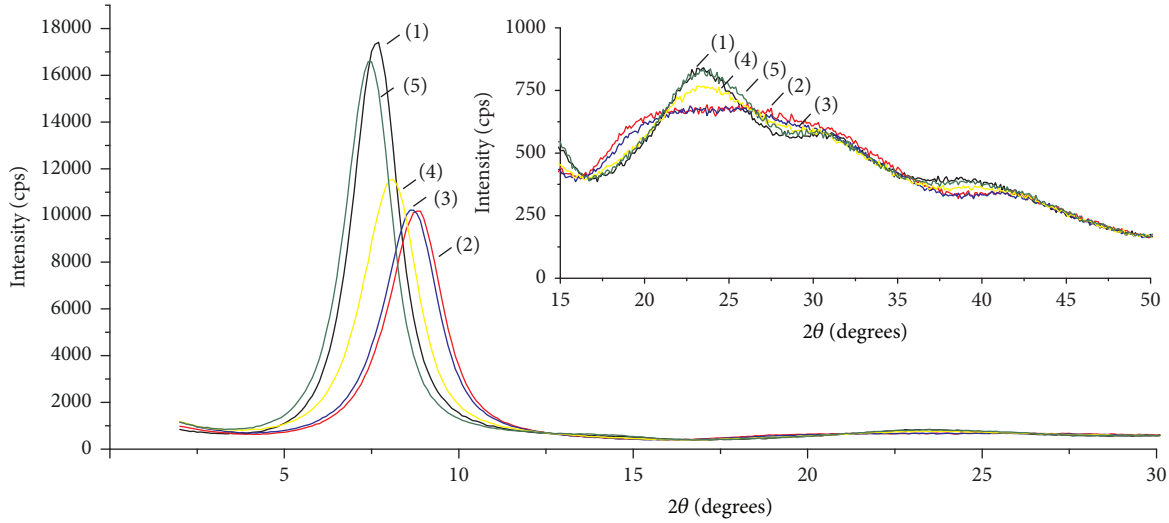

FIGURE 6: XRD patterns of V_2O_5 gel film: (1) initial; (2) 1 hour after hydrogenation; (3), (4), and (5) after 1, 7, and 14 days, respectively.

room temperature. Sample 2 (Figure 5) has been subjected to hydrogen implantation for 5 min at a pulse repetition rate of 2 kHz. A part of the sample has been covered with a mask during the plasma treatment; however, the temperature dependence of conductivity (curve (2) in Figure 5) shows that this part has also been hydrogenated with a small dose. Formula (1) yields a dose of $N = 7.5 \cdot 10^{16}$ cm^{-2} for sample 2, and the hydrogen concentration in the VO_2 film is thus $3.7 \cdot 10^{21}$ cm^{-3} (10.5 at.%). This value is much higher than that obtained in [18] (2 at.%). It has been stated [18] that metallization of VO_2 should occur when the hydrogen concentration in the film is equal to or higher than 4 at.%. Therefore, it may be assumed that PIII leads to metallization (curve (3) in Figure 5). This assumption also agrees with the data presented in [19] where vanadium dioxide nanobeams have been hydrogenated in the hydrogen flow.

Thus, it is demonstrated that the PIII technique allows one to perform hydrogenation of vanadium dioxide films and vary the concentration of hydrogen in the samples. Hydrogen is retained in the films for a long time, and the hydrogen concentration that is sufficient for metallization (i.e., for the metal tetragonal phase to be preserved at room temperature) is attained.

3.2. Vanadium Pentoxide Xerogel. The XRD analysis shows that the initial vanadium oxide film obtained by the sol-gel method is an amorphous $V_2O_5 \cdot nH_2O$ xerogel with n = 1.6–1.8. In Figure 6, the curves of X-ray scattering intensity distribution for the initial and hydrogenated films are presented.

Qualitatively, these curves are identical; that is, there are no sharp structural changes during hydrogenation in the films. However, the first maximum of the curve for the hydrogenated film is shifted toward larger angles as compared to that of the original sample, which indicates a decrease in the interlayer spacing (Table 2).

During the hydrogen implantation, the film is heated to about 100°C by radiation from the HCPS hot cathode. According to [20], at this temperature, a partial dehydration takes place—weakly bound water is reversibly removed

Table 2: Interlayer spacing (δ) calculated from the XRD data for the as-prepared, hydrogenated, and aged V_2O_5 xerogel films.

Sample	Number in Figure 6	2θ, °	δ, Å	I, cps
Initial film	(1)	7.65	11.55	11625
Hydrogenated	(2)	8.80	10.04	6805
1 day after hydrogenation	(3)	8.68	10.17	6850
1 week after hydrogenation	(4)	8.10	10.91	7744
2 weeks after hydrogenation	(5)	7.47	11.82	11082

($V_2O_5{\cdot}1.6H_2O \rightarrow V_2O_5{\cdot}0.5H_2O$), and the interlayer distance is reduced from 11.55 Å to 8.75 Å. Such a change of the interlayer distance by 2.8 Å corresponds to the disappearance of a monomolecular water layer. In our experiment, the interlayer distance, as a result of heating by hydrogenation, decreases by about 1.5 Å, down to 10.04 Å (Table 2), that is, for the time of hydrogenation, monomolecular layer of water is only partly extracted from the film.

At the electrochromic coloration of an initial (nonhydrogenated) film, analogous changes occur [13]. Here, partial dehydration is caused by the heating due to the current flow. However, the heating in that case is much less than the heating during the PIII-assisted hydrogenation, and therefore the interlayer distance decreases by only 0.65 Å.

The maxima at $2\theta \sim 23^\circ$, 32°, and 39.5° are diffuse due to the amorphous structure of the film. In the hydrogenated film, they slightly shift toward smaller angles and become even more blurred. This suggests that hydrogen is embedded into the structure of the V_2O_5 layers, which leads to an increase in atomic distances within the layers and to a decrease in the interlayer distance.

In order to track the recovery process, the XRD patterns of the film have also been obtained at 1, 7, and 14 days after hydrogenation (see Figure 6 and Table 2). In the hydrogenated films, the first peak shifts toward smaller angles with aging; that is, the interlayer distance gradually increases, reaching the value corresponding to the initial film and then even slightly exceeding it. This might indicate the process of hydrogen motion from the layers into the interlayer space with a possible formation of new water molecules, as well as the adsorption of water from air, since the films, because of their loose (amorphous and porous) structure, can rather easily absorb and desorb water.

For the Raman spectra measurements, the samples of crystalline V_2O_5 have been obtained by annealing of the xerogel films in a muffle furnace at a temperature of 400°C. According to the XRD data (Figure 7), the annealed film contains 90% of crystalline V_2O_5, about 10% of amorphous $V_2O_5{\cdot}1.6H_2O$, and small amount of VO_2. The spectra of the samples (Figure 8) are qualitatively similar to the data on Raman scattering of vanadium pentoxide reported in the literature [21–23]. A peak at 932 cm^{-1} corresponding to the V^{4+}=O bonds is reported in the work [23], and it is not observed in our samples. Note however that a band around 900 cm^{-1} appears to slightly rise above the background of the hydrogenated film spectrum (curve (2) in the insert of Figure 8), which might indicate some V^{4+} concentration increase.

For the study of the influence of hydrogenation (with the dose of $N \approx 10^{17}$ cm^{-2}) on the IECE, the samples partially covered by a mask during the hydrogenation process have been used. The colored spot growth rate at different arrangement of electrodes is shown in Figure 9.

The colored spot can persist up to 24 hours, and when applying the reverse voltage, the spot disappears for 1–5 minutes. The films withstand up to 10^4 coloring-bleaching cycles. From Figure 9, one can see that when the negative electrode is located on the nonhydrogenated part of the film and the positive electrode on the hydrogenated part (i.e., if the nonhydrogenated region is colored), the IECE is more pronounced, while at the reverse polarity, the effect is practically suppressed. This is accounted for by the fact that in the former case the migration of protons from the region enriched with hydrogen is substantially enhanced, and in the latter case, at the reverse polarity, the migration is impeded.

Next we have studied the optical properties of the hydrogenated and colored samples. The $R(\lambda)$ and $T(\lambda)$ spectra are shown in Figure 10. The transmittance (Figure 10(b)) increases at electrochromic coloration and falls at hydrogenation. The film reflectance (Figure 10(a)) increases both at coloration and at hydrogenation, though the rise of R is greater in the red wavelength (over 650 nm) spectrum region after electrochromic coloration, while after hydrogenation it is greater in the blue and green wavelength region (400–550 nm). We recall that, at the electrochromic effect, the color of the film is bright red, and the hydrogenation results in the dark-green film color.

The optical bandgap E_g has been estimated on the assumption of allowed direct transitions [13]:

$$(\alpha h\nu)^2 = A\left(h\nu - E_g\right), \tag{2}$$

where A is a constant, h is the Planck constant, $\nu = c/\lambda$ (with c being the light velocity) is the photon frequency, and α is the absorption coefficient calculated from (3) based on the obtained spectral dependence of T and R and the film thickness (d):

$$\alpha = \frac{1}{d} \ln \frac{(1-R)^2}{T}. \tag{3}$$

From these measurements, the optical bandgap has been found to be $E_g = (2.30 \pm 0.05)$. A decrease in the value of E_g at the IECE, by approximately 0.05–0.1 eV, is observed both in the as-prepared films and in those exposed to hydrogenation. Structural changes occurring in the films at the proton concentration increase might account for these E_g

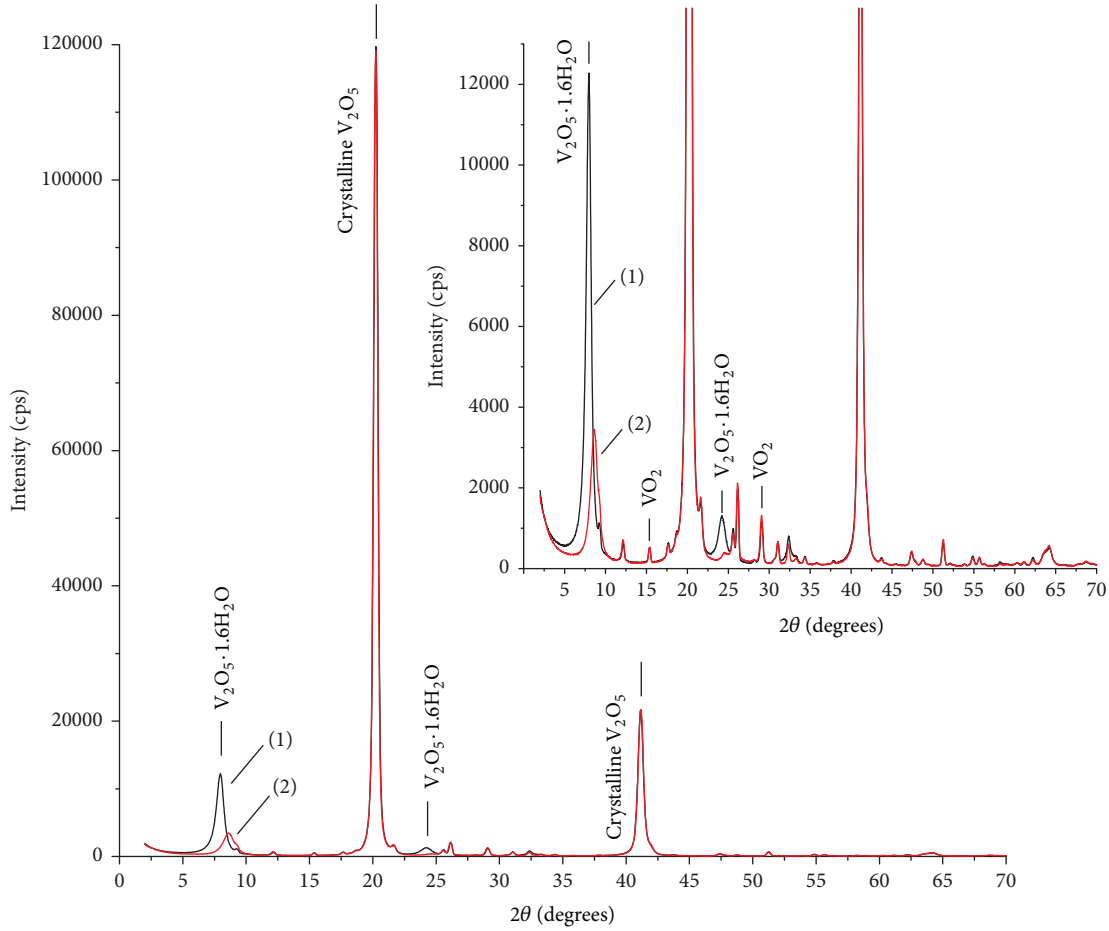

FIGURE 7: XRD patterns of $V_2O_5{\cdot}nH_2O$ film annealed at 400°C (1) and that same film hydrogenated after annealing (2). For curve (1), the peaks corresponding to crystalline V_2O_5 coincide with the peaks of curve (2).

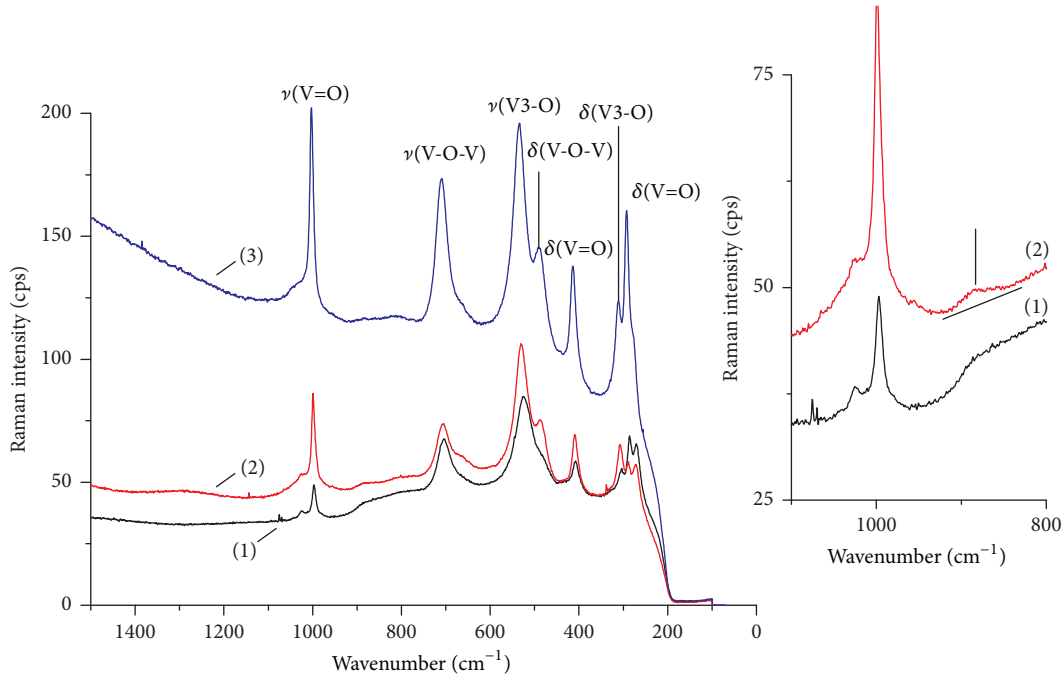

FIGURE 8: Raman spectra of crystalline V_2O_5: (1) initial film, (2) hydrogenated region, and (3) region colored at the IECE. Specific bending (δ) and stretching (ν) vibration modes from the works [21–23] are indicated.

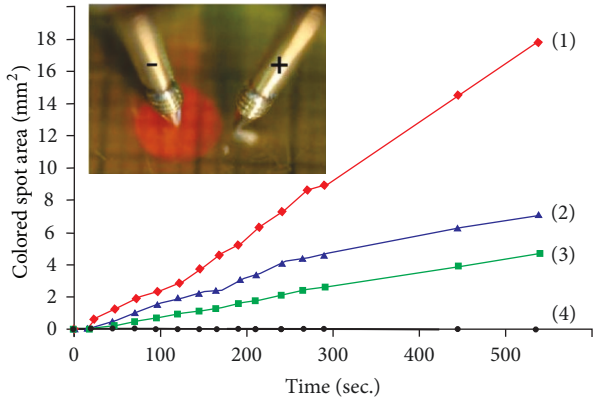

FIGURE 9: Colored spot area as a function of time of voltage application: (1) the negative electrode is located on nonhydrogenated region and the positive one on hydrogenated region (see insert); (2) both electrodes are on as-prepared (nonhydrogenated) film; (3) both electrodes are on hydrogenated film; (4) the negative electrode is located on hydrogenated region, and the positive one on initial film.

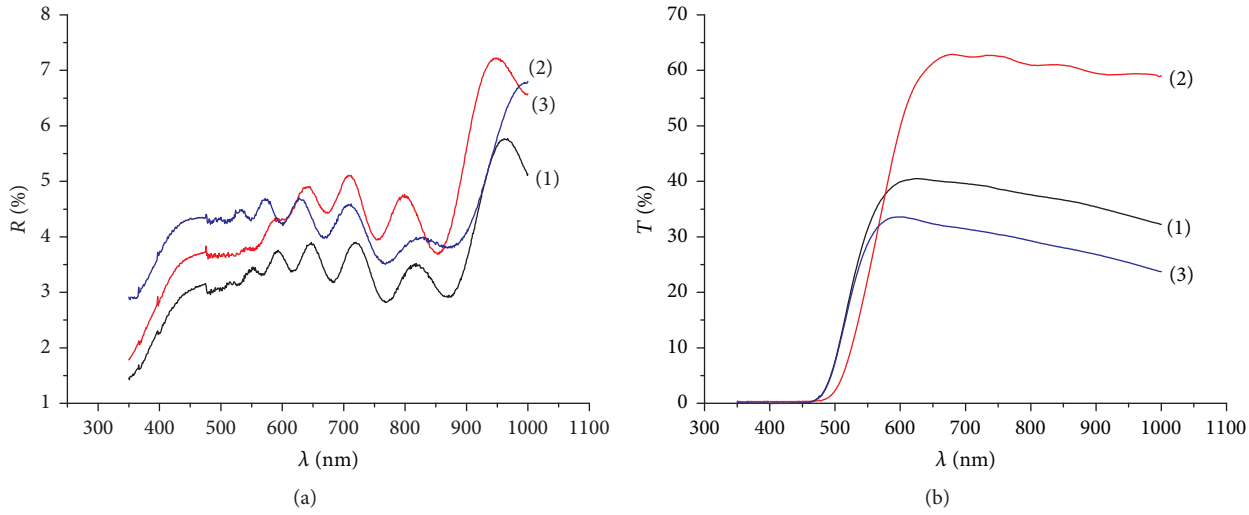

FIGURE 10: Reflectance (a) and transmittance (b) spectra of V_2O_5 xerogel film: (1) initial film, (2) colored region, and (3) hydrogenated region.

changes [13]. At the electrochromic coloration of the as-prepared films, this proton concentration increase is due to the migration of hydrogen ions to the negatively charged electrode, while at plasma treatment it is due to the hydrogen implantation.

^{51}V MAS NMR spectra of both initial and hydrogenated films (Figure 11(a)) contain the only signal with isotropic shift around −575 ppm, which corresponds to vanadium in the vanadium pentoxide phase of V_2O_5-xerogel [24]. However, the intensity of the signal in hydrogenated film is lower by 2.7 times than in initial one. Most likely, the plasma treatment results in a partial reduction of V^{+5} to V^{+4} oxidation state, which is paramagnetic and invisible in NMR spectra, and leads to the corresponding decrease of the NMR signal intensity. Also, an additional decrease of the signal from V^{+5} in the MAS NMR spectra recorded by the Hahn echo technique can be caused by a decrease of relaxation times of V^{5+} ions which are located close to V^{4+}. The increased width of the lines in the ^{51}V MAS NMR spectrum of the hydrogenated film has the same reason.

The partial $V^{5+} \rightarrow V^{4+}$ reduction seems to be supported by the 900 cm^{-1} Raman peak intensity increase (Figure 8, insert). That is why, apparently, electrochromic coloration does not occur in the hydrogenated region, because the formation of highest polyvanadic acids is hindered there. The fact is that the film coloration to red color is accounted for by the formation of highest polyvanadic acids, where the vanadium oxidation state is +5. At the PIII-induced hydrogenation, the pentavalent vanadium concentration reduces; therefore, the formation of hexa- and decavanadic acids is hindered, and the coloration no longer occurs in the hydrogenated region.

To further affirm this inference, we have conducted an additional experiment, namely, tested another method of hydrogenation, by holding the sample in hot (125°C) glycerin. Heating causes the decomposition of glycerin to form glycerol aldehyde and molecular hydrogen [25].

Provided that the formed hydrogen gas can not escape through the surface, it turns out to be dissolved in liquid glycerin. If some hydrogen molecule decomposition catalyst (e.g.,

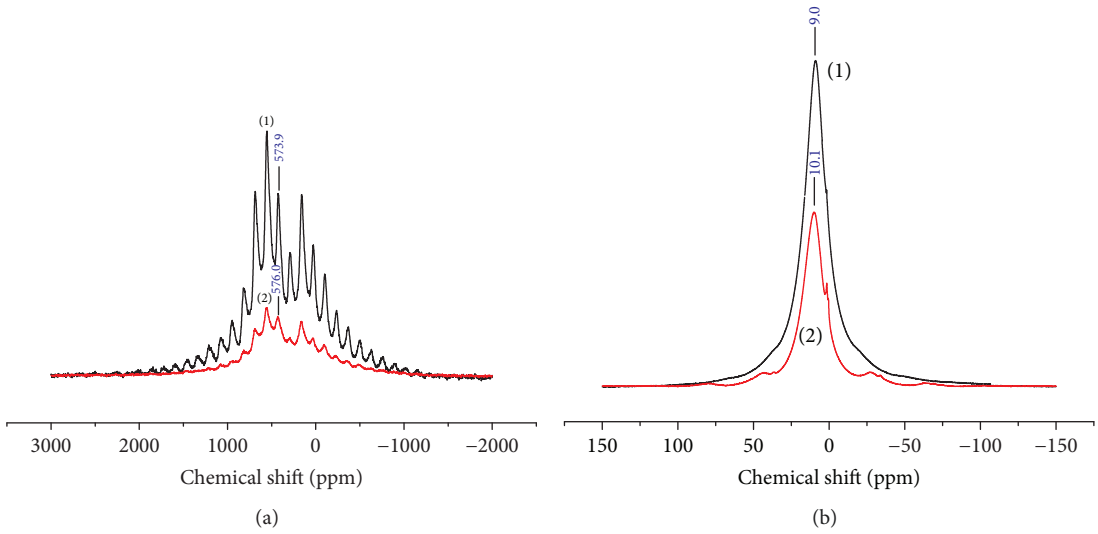

Figure 11: (a) ^{51}V MAS NMR spectra. Not marked signals are spinning sidebands. (b) ^{1}H MAS NMR spectra. (1) Initial film; (2) hydrogenated film.

vanadium pentoxide) is present in the reaction chamber, then atomic hydrogen appears and penetrates into the V_2O_5 film where it splits into protons and electrons. The vanadium pentoxide film changes its color from brown to blue-green. However, in this case, no changes occur in the concentration of pentavalent vanadium. The internal electrochromic effect in the film hydrogenated by such a way is much brighter than that in the nonhydrogenated film. Unfortunately, this method of the IECE enhancement can hardly be applied in practice because of an uncontrollable film delamination from the substrate during the hot glycerin treatment. Nonetheless, this experiment proves that the IECE manifestation after hydrogenation depends not solely on hydrogen excess, but primarily on the vanadium valence state.

In the ^{1}H MAS NMR spectra (Figure 11(b)), the only signal at 9-10 ppm is also observed for both the films. We suppose that it corresponds to a proton in an H_3O^+ ion formed by the interaction of water molecules with acidic protons of polyvanadic acid. The high water content in the material (around 15% in the initial state) makes it impossible to observe protons in other surroundings, including hydrogen introduced by hydrogenation. During the hydrogenation procedure, two opposing processes take place changing the content of protons in the film. The heating of the film at 100°C removes the water and corresponding protons. The hydrogenation, on the contrary, introduces the hydrogen into the film. However, the addition of hydrogen ions from plasma is far from being able to compensate the loss of hydrogen due to the water removal. This fact is confirmed by the ^{1}H MAS NMR measurements. After the treatment, the number of protons in the film (integral intensity of ^{1}H MAS NMR spectra) is about 65% of the initial value. In addition, this conclusion is further confirmed by the TGA data presented in Figure 12.

From the results of TGA (Figure 12), one can see that the sample mass loss at 100°C for 30 minutes is about 10.8%, and at 400°C it is about 15%, which corresponds to the total removal of the initial interlayer water. Thus, we can conclude that, at the hydrogen implantation into a V_2O_5 xerogel film, approximately 72% of the interlayer water leaves the sample. As a result of implantation with a dose of $3.5 \cdot 10^{17}$ cm^{-2}, $\sim 5.4 \cdot 10^{17}$ ions with a total mass of $9 \cdot 10^{-5}$ g are added to the film. For the 0.05 g mass of the V_2O_5 xerogel film, it is straightforward to calculate that, from the TGA data and taking into account the implanted hydrogen, the hydrogen content in the films after implantation is about 39% of the initial quantity, which agrees qualitatively with the above value obtained from the NMR measurements.

Thus, the TGA results are consistent with the ^{1}H NMR data. The total amount of hydrogen decreases after implantation. However, the implanted hydrogen differs from the hydrogen composed in water. First of all, the implanted hydrogen is not bound in the film; that is, it possesses a higher mobility. Perhaps this explains the enhancement of the electrochromic effect in $V_2O_5 \cdot nH_2O$ films when the negative electrode is located on the nonhydrogenated region and the positive one on hydrogenated region.

In summary we have studied the internal electrochromic effect in vanadium pentoxide xerogel film and the influence of hydrogenation on its parameters. The PIII-assisted hydrogen insertion has been found to benefit the coloration rate at a specific mutual arrangement of electrodes. Particularly, if the negative electrode is located on the nonhydrogenated region and the positive electrode on the hydrogenated one, the IECE is more pronounced, while at the reverse polarity (or if both electrodes are on hydrogenated region), the IECE is practically suppressed. This is associated with the fact that the migration of protons from the region enriched with hydrogen is substantially enhanced, while it is impaired at the reverse polarity.

The ^{51}V MAS NMR analysis and Raman spectroscopy have revealed a partial reduction of V^{5+} to V^{4+} oxidation

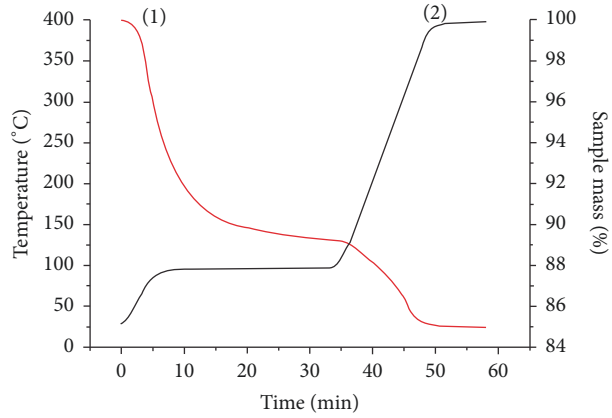

FIGURE 12: TGA of $V_2O_5 \cdot 1.8H_2O$: (1) sample mass; (2) temperature.

state at hydrogenation. This accounts for the fact that electrochromic coloration does not occur in the hydrogenated region, because the formation of highest polyvanadic acids, responsible for the $V_2O_5 \cdot nH_2O$ electrochromic coloration, is hindered there due to a decrease in the pentavalent vanadium concentration. In addition, it has been shown that, unlike the PIII hydrogenation, the hydrogenation in glycerin results in the IECE enhancement in the hydrogenated region, albeit hydrogen is added to the material in both cases. The difference in these two hydrogenation methods consists precisely in the fact that the former one leads to a decrease in the V^{5+} concentration, whereas the latter method does not change this concentration. Finally, according to the ^1H NMR and TGA data, the total amount of hydrogen decreases after implantation due to the heat-induced water loss. However, the implanted hydrogen differs from the hydrogen composed in water because it is not bound in the film and possesses a higher mobility. That is why the internal electrochromic effect in $V_2O_5 \cdot nH_2O$ films is enhanced after plasma-immersion hydrogen ion implantation.

3.3. Switching in MOM Structures Based on Hydrated Vanadium Pentoxide. Electrical switching due to MIT has been first revealed for vanadium dioxide [7].

Switching in VO_2 is associated with the current-induced Joule heating of the sample up to $T = T_t$. The switching effect has been observed in vanadium dioxide single crystals and thin-film structures of both planar and sandwich-type [1, 5, 7], as well as in vanadate-phosphate glasses [26], VO_2-containing ceramics [27], and V_2O_5-gel films [8, 28]. When as-prepared samples do not consist of pure vanadium dioxide, preliminary electrical forming (EF) is required, resulting in formation of the VO_2-containing channel [7, 8, 26–28].

In our experiments, after EF in the film of pure hydrated vanadium pentoxide, a vanadium dioxide channel forms where the MIT can occur. The current-voltage characteristic of the structure becomes S-shaped with $V_{th} \approx 2$ V. Thus, a stable switching structure is formed with a sufficiently large resistance jump (of up to two orders of magnitude) in the *I-V* curve (Figure 13).

Implantation of tungsten greatly influences the *I-V* curves of the switching structures. For the $V_2O_5 \cdot 1.8H_2O$ film after implantation of $W(CO)_6$ for 1 minute (the W content in the film, according to the EDX spectroscopy data, is ~0.4 at.%), the conductivity jump, when switching from the high-resistance off state to the low-resistance on state, is greater than that in the original film (Figure 14(a)). Moreover, the switching parameters scatter is significantly lower than that in the initial films without implantation. This might indicate that the admixture of tungsten reduces the scatter due to a decrease of the MIT temperature caused by W doping [8]. For the $V_2O_5 \cdot 1.8H_2O$ film after implantation of $W(CO)_6$ for 5 minutes (the W concentration is ~7 at.%), switching in sandwich structures without a preliminary EF is observed (Figure 14(b)). At the same film after EF, the conduction jump disappears completely, and the channel transits into the metallic state (Figure 14(c)).

Note that the doping with metal ions has a profound influence on the phase transition behavior and transition temperature of VO_2 [9]. Particularly, the substitution of V^{4+} ions with metal-ion dopants of higher oxidation states, such as W^{6+} or Nb^{5+}, lowers the transition temperature. Moreover, doping of VO_2 with tungsten up to 14 at.% results in its metallization [1], and, according to recent data [29], metallization occurs at even lower W concentration, about 9.5 at.%. It is to be noted that, as is shown in Section 3.1, the doping of vanadium dioxide films with large doses of hydrogen by PIII also results in the film metallization.

One can assume that for a high W implantation dose a transformation of vanadium pentoxide xerogel into VO_2, brought about by heating and ion bombardment, occurs simultaneously with doping. That is, in this case some amount of VO_2 : W might be formed at plasma treatment. That is why no preliminary EF is required, and the resistivity jump at switching decreases: compare *I-V* curves in Figures 14(a) and 14(b). During electrical forming, additional doping of the channel with tungsten is possible due to the W ions electromigration. If the W content is increased from 7 to 9.5 at.%, then the W-doped VO_2 channel becomes metallic and switching no longer occurs in such a sample (Figure 14(c)). Also, the observed degeneracy of the *I-V* characteristic might be associated with the fact that in this case a conventional electrical breakdown occurs instead of electrical forming [7]. Unfortunately, it turned out to be impossible to confirm

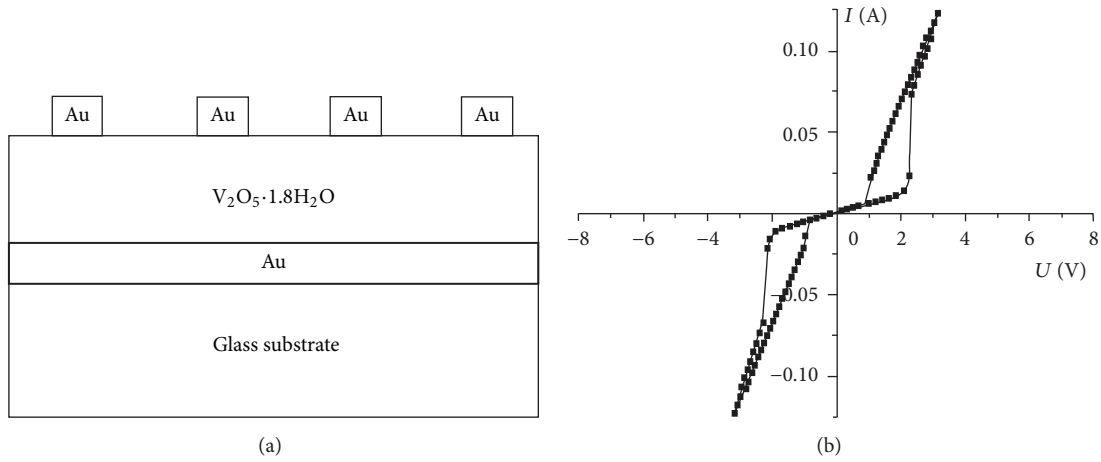

Figure 13: (a) Schematic sandwich structure: diameter of Au top electrodes is 0.9 mm. (b) *I-V* curve after EF.

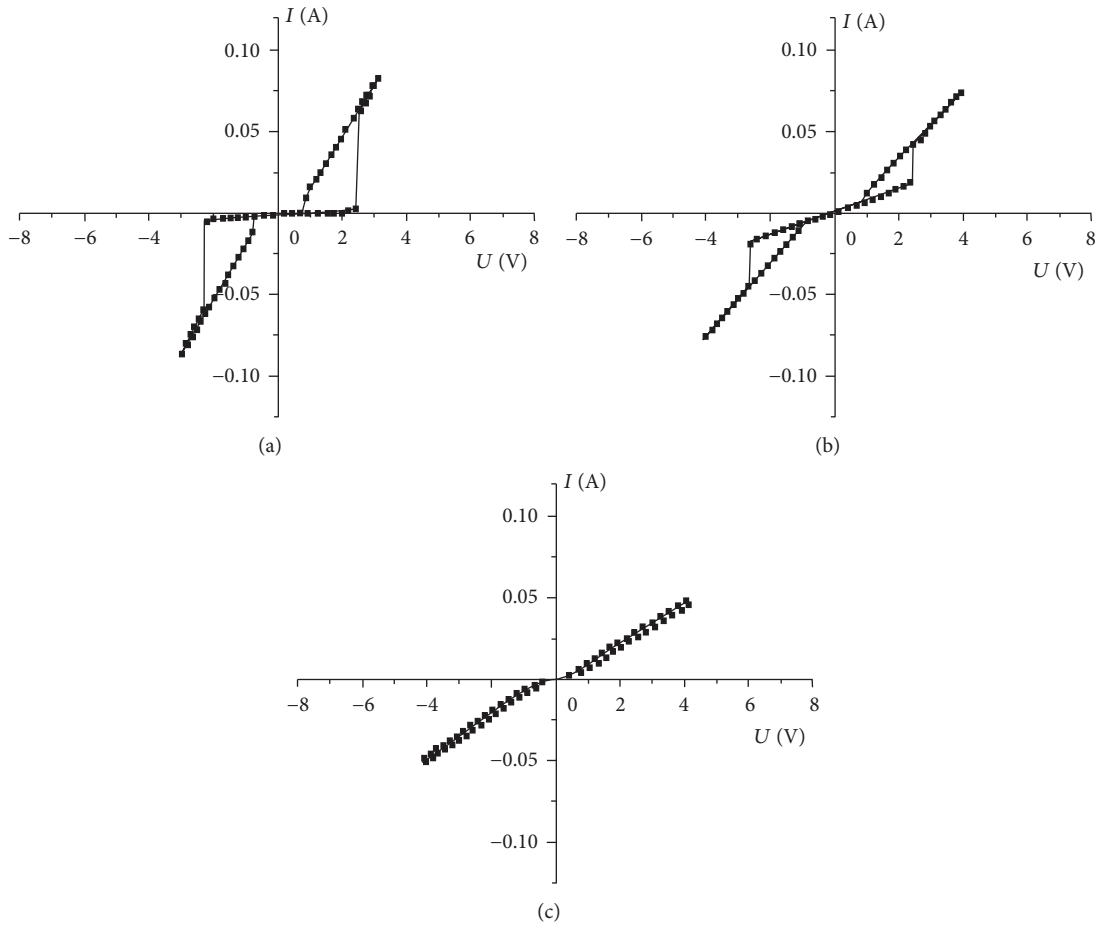

Figure 14: (a) *I-V* curves of the $V_2O_5 \cdot 1.8H_2O$ based MOM structures: (a) after W implantation for 1 min, electroformed; (b) after W implantation for 5 min, not electroformed; (c) after W implantation for 5 min, electroformed.

the above made assumption (concerning the VO_2 formation during PIII of W) using, for example, XRD analysis because of the complex mixture of phases which are difficult to identify. Nonetheless, we recall that a similar situation takes place at PIII of hydrogen where a partial $V^{5+} \rightarrow V^{4+}$ reduction does occur.

Thus, the implantation of small doses of tungsten into vanadium pentoxide films significantly improves their switching parameters. When implanting relatively large doses, the switching effect is observed without a preliminary electroforming process, but in case of EF, switching vanishes due to either metallization or breakdown.

4. Conclusion

In this paper, we have studied the effect of doping with hydrogen and tungsten on the properties of vanadium dioxide and hydrated vanadium pentoxide films. For carrying out the efficient doping process, the plasma-immersion ion implantation method has been developed and implemented.

It is shown that the implantation of hydrogen by the PIII method in vanadium dioxide films leads to the suppression of the MIT and, at a hydrogen concentration greater than 10.5 at.%, to the VO_2 metallization at $T < T_t$. This inference is in agreement with the data available in the literature [10, 18, 19, 25]. In addition, hydrogen is retained in the films for a long time.

Also in this study the internal electrochromic effect in $V_2O_5{\cdot}nH_2O$ films, as well as its modification under the PIII-assisted hydrogenation, has been examined. It is shown that when the negative electrode is located on the nonhydrogenated region of the film and the positive electrode on the hydrogenated region, the IECE is more pronounced. This is accounted for by the fact that the migration of protons from the region enriched with hydrogen is substantially enhanced.

Thus, we conclude that a method has been found for substantial increase of the rate of electrochromic coloring of hydrated vanadium pentoxide films without the use of an electrolyte. The observed phenomenon can find application in various electrochromic devices [11, 13], such as electrochromic coatings for smart windows.

Next we have studied the switching effect in the metal-$V_2O_5{\cdot}nH_2O$-metal structures. It is shown that the implantation of small doses of tungsten into vanadium pentoxide films significantly improves their switching parameters. When implanting relatively large doses, the switching effect is observed without preliminary electroforming, but in case of EF switching vanishes.

Finally, we would like to comment on the doping method used in the present study. As has been shown in the review [14], "PIII is a cluster compatible doping and processing tool offering many inherent advantages over conventional beamline ion implantation... Recently, a substantial amount of research activities have focused on microelectronics and have led to a number of very interesting applications, such as the formation of shallow junction, synthesis of silicon-on-insulator, large area implantation, trench doping, conformal deposition, and so on." We add that lately the PIII technique has successfully been applied for the synthesis of biocompatible materials, see, for example, the paper [30]. The results presented above show that, owing its advantages, PIII can be used for doping vanadium oxides with hydrogen and metals in order to modify their properties.

Conflicts of Interest

The authors declare that they have no conflicts of interest.

Acknowledgments

This work was supported by the RF Ministry of Education and Science, Project no. 16.5857.2017/8.9 (state program), and by the Flagship University Development Program of Petrozavodsk State University (2017–2021). The authors thank Yu. Kolyagin and L. Lugovskaya for their help with NMR (Yu. Kolyagin) and XRD (L. Lugovskaya) measurements and useful discussions.

References

[1] A. A. Bugaev, B. P. Zakharchenya, and F. A. Chudnovskii, *Metal-Semiconductor Phase Transition and Its Applications*, Nauka, Leningrad, Russia, 1979.

[2] A. L. Pergament, G. B. Stefanovich, N. A. Kuldin, and A. A. Velichko, "On the problem of metal-insulator transitions in vanadium oxides," *ISRN Condensed Matter Physics*, vol. 2013, Article ID 960627, 6 pages, 2013.

[3] C. Lamsal and N. M. Ravindra, "Optical properties of vanadium oxides-an analysis," *Journal of Materials Science*, vol. 48, no. 18, pp. 6341–6351, 2013.

[4] R. Jaramillo, S. D. Ha, D. M. Silevitch, and S. Ramanathan, "Origins of bad-metal conductivity and the insulator-metal transition in the rare-earth nickelates," *Nature Physics*, vol. 10, no. 4, pp. 304–307, 2014.

[5] A. Pergament, P. Boriskov, N. Kuldin, and A. Velichko, "Electrical conductivity of vanadium dioxide switching channel," *Physica Status Solidi B* , vol. 247, no. 9, pp. 2213–2217, 2010.

[6] T. J. Huffman, C. Hendriks, E. J. Walter et al., "Insulating phases of vanadium dioxide are Mott-Hubbard insulators," *Physical Review B: Condensed Matter and Materials Physics*, vol. 95, no. 7, Article ID 075125, 2017.

[7] A. Pergament, G. Stefanovich, V. Malinenko, and A. Velichko, "Electrical switching in thin film structures based on transition metal oxides," *Advances in Condensed Matter Physics*, vol. 2015, Article ID 654840, 26 pages, 2015.

[8] O. Y. Berezina, A. A. Velichko, L. A. Lugovskaya, A. L. Pergament, and G. B. Stefanovich, "Metal-semiconductor transition in nonstoichiometric vanadium dioxide films," *Inorganic Materials*, vol. 43, no. 5, pp. 505–511, 2007.

[9] W.-K. Hong, S. N. Cha, J. I. Sohn, and J. M. Kim, "Metal-Insulator Phase Transition in Quasi-One-Dimensional VO_2 Structures," *Journal of Nanomaterials*, vol. 2015, Article ID 538954, 15 pages, 2015.

[10] H. Yoon, M. Choi, T.-W. Lim et al., "Reversible phase modulation and hydrogen storage in multivalent VO_2 epitaxial thin films," *Nature Materials*, vol. 15, no. 10, pp. 1113–1119, 2016.

[11] N. A. Chernova, M. Roppolo, A. C. Dillon, and M. S. Whittingham, "Layered vanadium and molybdenum oxides: batteries and electrochromics," *Journal of Materials Chemistry*, vol. 19, no. 17, pp. 2526–2552, 2009.

[12] A. I. Gavrilyuk and F. A. Chudnovskii, "Electrochromism in vanadium pentoxide films," *Technical Physics Letters*, vol. 3, no. 1, pp. 69-70, 1977.

[13] D. Yakovleva, A. Pergament, O. Berezina, P. Boriskov, D. Kirienko, and V. Pikulev, "Internal electrochromism in vanadium pentoxide xerogel films," *Materials Science in Semiconductor Processing*, vol. 44, pp. 78–84, 2016.

[14] P. K. Chu, S. Qin, C. Chan, N. W. Cheung, and L. A. Larson, "Plasma immersion ion implantation - A fledgling technique for semiconductor processing," *Materials Science and Engineering: R: Reports*, vol. 17, no. 6-7, pp. 207–280, 1996.

[15] J.-J. Legendre and J. Livage, "Vanadium pentoxide gels:. i. structural study by electron diffraction," *Journal of Colloid and Interface Science*, vol. 94, no. 1, pp. 75–83, 1983.

[16] V. N. Andreev and V. A. Klimov, "Effect of the metal-semiconductor phase transition on the rate of hydrogen penetration into vanadium dioxide thin films," *Physics of the Solid State*, vol. 52, no. 3, pp. 605–611, 2010.

[17] S. V. Burdyukh, G. B. Stefanovich, A. L. Pergament, O. Y. Berezina, N. A. Avdeev, and A. B. Cheremisin, "Modification of the properties of vanadium dioxide by plasma-immersion ion implantation," *Technical Physics Letters*, vol. 42, no. 1, pp. 32–35, 2016.

[18] V. N. Andreev, V. A. Klimov, and M. E. Kompan, "Influence of hydrogenation on electrical conductivity of vanadium dioxide thin films," *Physics of the Solid State*, vol. 54, no. 3, pp. 601–606, 2012.

[19] J. Lin, H. Ji, M. W. Swift et al., "Hydrogen diffusion and stabilization in single-crystal VO2 Micro/Nanobeams by direct atomic hydrogenation," *Nano Letters*, vol. 14, no. 9, pp. 5445–5451, 2014.

[20] P. Barboux, N. Baffier, R. Morineau, and J. Livage, "Diffusion protonique dans les xerogels de pentoxyde de vanadium," *Solid State Ionics*, vol. 9-10, no. 2, pp. 1073–1080, 1983.

[21] C. Sanchez, J. Livage, and G. Lucazeau, "Infrared and raman study of amorphous V_2O_5," *Journal of Raman Spectroscopy*, vol. 12, no. 1, pp. 68–72, 1982.

[22] M. Castriota, E. Cazzanelli, A. Fasanella, and D. Teeters, "Electrical conductivity and Raman characterization of V_2O_5 grown by sol-gel technique inside nanoscale pores," *Thin Solid Films*, vol. 553, pp. 127–131, 2014.

[23] S.-H. Lee, H. M. Cheong, M. Je Seong et al., "Microstructure study of amorphous vanadium oxide thin films using raman spectroscopy," *Journal of Applied Physics*, vol. 92, no. 4, pp. 1893–1897, 2002.

[24] C. J. Fontenot, J. W. Wiench, M. Pruski, and G. L. Schrader, "Vanadia gel synthesis via peroxovanadate precursors. 2: Characterization of the gels," *The Journal of Physical Chemistry B*, vol. 105, no. 43, pp. 10496–10504, 2001.

[25] A. V. Ilinskiy, O. E. Kvashenkina, and E. B. Shadrin, "Protonic metallization of the monoclinic phase in VO_2 films," *Semiconductors*, vol. 45, no. 9, pp. 1153–1157, 2001.

[26] V. N. Andreev, N. E. Timoschenko, I. M. Chernenko, and F. A. Chudnovskii, "Mechanism of formation of switching vanadate phosphate glasses," *Journal of Technical Physics*, vol. 51, no. 8, pp. 1685–1689, 1981.

[27] A. I. Ivon, V. R. Kolbunov, and I. M. Chernenko, "Voltage-current characteristics of vanadium dioxide based ceramics," *Journal of the European Ceramic Society*, vol. 23, no. 12, pp. 2113–2118, 2003.

[28] J. G. Zhang and P. C. Eklund, "The switching mechanism in V_2O_5 gel films," *Journal of Applied Physics*, vol. 64, no. 2, pp. 729–733, 1988.

[29] K. Shibuya, M. Kawasaki, and Y. Tokura, "Metal-insulator transition in epitaxial $V_{1-x}W_xO_2$ ($0 < x < 0.33$) thin films," *Appl. Phys. Lett*, vol. 96, Article ID 022102, 2010.

[30] C. Zietz, A. Fritsche, B. Finke et al., "Analysis of the release characteristics of Cu-treated antimicrobial implant surfaces using atomic absorption spectrometry," *Bioinorganic Chemistry and Applications*, vol. 2012, Article ID 850390, 5 pages, 2012.